

## Article

# Angle-Dependent Magic Optical Trap for the $6S_{1/2} \leftrightarrow nP_{3/2}$ Rydberg Transition of Cesium Atoms

Jiandong Bai <sup>1,2</sup> , Xin Wang <sup>2</sup>, Xiaokai Hou <sup>2</sup>, Wenyuan Liu <sup>1</sup> and Junmin Wang <sup>2,3,\*</sup> 

<sup>1</sup> Department of Physics, North University of China, Taiyuan 030051, China; jdbai@nuc.edu.cn (J.B.); liuweny@nuc.edu.cn (W.L.)

<sup>2</sup> State Key Laboratory of Quantum Optics and Quantum Optics Devices, and Institute of Opto-Electronics, Shanxi University, Taiyuan 030006, China; 2019122607014@email.sxu.edu.cn (X.W.); 201922607008@email.sxu.edu.cn (X.H.)

<sup>3</sup> Collaborative Innovation Center of Extreme Optics, Shanxi University, Taiyuan 030006, China

\* Correspondence: wwjjmm@sxu.edu.cn

**Abstract:** The existence of an anisotropic tensor part of atomic states with an angular momentum greater than 1/2 causes their dynamic polarizabilities to be very sensitive to the polarization direction of the laser field. Therefore, the magic wavelength of the transition between two atomic states also depends on the polarization angle between the quantized axis and the polarization vector. We perform a calculation of the magic conditions of the  $6S_{1/2} \leftrightarrow nP_{3/2}$  ( $n = 50-90$ ) Rydberg transition of cesium atoms by introducing an auxiliary electric dipole transition connected to the target Rydberg state and a low-excited state. The magic condition is determined by the intersection of dynamic polarizabilities of the  $6S_{1/2}$  ground state and the  $nP_{3/2}$  Rydberg state. The dynamic polarizability is calculated by using the sum-over-states method. Furthermore, we analyze the dependence of magic detuning on the polarization angle for a linearly polarized trapping laser and establish the relationship between magic detuning and a principal quantum number of the Rydberg state at the magic angle. The magic optical dipole trap can confine the ground-state and Rydberg-state atoms simultaneously, and the differential light shift in the  $6S_{1/2} \leftrightarrow nP_{3/2}$  transition can be canceled under the magic condition. It is of great significance for the application of long-lifetime high-repetition-rate accurate manipulation of Rydberg atoms on high-fidelity entanglement and quantum logic gate operation.

**Keywords:** Rydberg atoms; dynamic polarizability; optical dipole trap; magic trapping; polarization angle



**Citation:** Bai, J.; Wang, X.; Hou, X.; Liu, W.; Wang, J. Angle-Dependent Magic Optical Trap for the  $6S_{1/2} \leftrightarrow nP_{3/2}$  Rydberg Transition of Cesium Atoms. *Photonics* **2022**, *9*, 303.

<https://doi.org/10.3390/photonics9050303>

Received: 12 April 2022

Accepted: 27 April 2022

Published: 28 April 2022

**Publisher's Note:** MDPI stays neutral with regard to jurisdictional claims in published maps and institutional affiliations.



**Copyright:** © 2022 by the authors. Licensee MDPI, Basel, Switzerland. This article is an open access article distributed under the terms and conditions of the Creative Commons Attribution (CC BY) license (<https://creativecommons.org/licenses/by/4.0/>).

## 1. Introduction

Rydberg atoms in highly excited states have many exaggerated properties [1], such as a long radiation lifetime, a large electric dipole moment, and so on, which make it an attractive medium for scalable quantum simulation and quantum computing [2–4]. On account of the strong controllable interactions among Rydberg atoms, researchers have successfully realized single-photon sources [5,6], single-photon transistors [7], two- and three-bit quantum gates [8,9], and quantum simulations of spin models in optical lattices. In the above most experiments about the optical trapping and coherent manipulation of cold Rydberg atoms, the conventional red-detuned optical dipole traps (ODTs) can only capture the ground-state atom to realize spatial localization [10], but it is a barrier to eject Rydberg atoms out of the trap. Therefore, it is necessary to turn off the light trap during the preparation and manipulation of Rydberg atoms. Due to the limited atomic temperature, the fidelity of the quantum state and the available time of coherent dynamics are only tens of microseconds, which is much lower than the spontaneous radiation lifetime of hundreds of microseconds of the Rydberg state. It will result in a low experiment repetition rate, especially in the quick decoherence by atomic thermal diffusion.

For the applications of quantum technology based on Rydberg atoms, it is crucial that the atoms can be trapped and manipulated precisely. Although it has been demonstrated that Rydberg atoms can be effectively captured by a magnetic field-induced Zeeman effect [11,12] and an electric-field-induced Stark effect [13], the structure of these potential wells is relatively complex and difficult to operate, and the manipulation of atoms can only be achieved at the millimeter level. In recent years, researchers have attempted to manipulate Rydberg atoms by means of the light trap with micron-level precision. Since the highly excited Rydberg atomic size is larger than the conventional optical lattice constants in general, the nearly free valence electrons undergo a pondermotive potential. Therefore, Rydberg atoms can be captured by trapping its electrons due to the coulomb interaction between electrons and nuclei. In 2011, the trapping of  $^{87}\text{Rb}$  Rydberg atoms was experimentally demonstrated in a one-dimensional pondermotive optical lattice by rapidly reversing the potential [14]. However, the experimental configuration is complicated and the confined Rydberg atoms have a short lifetime. Recently, the three-dimensional trapping of the  $nS_{1/2}$  ( $n = 60\text{--}90$ ) Rydberg state [15] and the Rydberg circular state [16] of  $^{87}\text{Rb}$  atoms in a bottle light trap have been realized by taking full advantage of the repulsive potential of conventional light trap to Rydberg atoms. The trapping lifetime of Rydberg atoms is extended because the atoms are confined in the minimum light intensity and the photon scattering is smaller. However, the simultaneous trapping of ground-state and Rydberg-state atoms has not been achieved in the above experiments.

Magic-wavelength ODT is constructed by the so-called magic-wavelength laser beam in pre-cooled atoms [17], at which the light shifts of the ground state and the target excited state are exactly the same. Therefore, the ground-state and excited-state atoms can be simultaneously trapped in the magic-wavelength ODT, and the spatial position-dependent differential light shift of the transition between the two states can be completely eliminated. At present, it has become a powerful tool for the manipulation of cold atoms, especially the coherent manipulation of atomic states. Additionally, it plays an important role in the fields of ultra-stable optical lattice clocks, long-life quantum memory, and precise manipulation of ultra-cold molecules. Since the application of magic-wavelength ODT trapping technology in Rydberg states of alkali metal atoms is challenging [18–21], the ordinary magic-wavelength ODTs are mainly used to the trapping of ground-state and low excited-state atoms [22,23].

In this paper, we investigate a magic ODT for the  $6S_{1/2} \leftrightarrow nP_{3/2}$  single-photon Rydberg transition of Cs atoms, which can cancel the differential light shift of the transition by introducing an auxiliary state. The magic condition is determined by the intersect point of dynamic polarizabilities of the  $6S_{1/2}$  ground state and the  $nP_{3/2}$  Rydberg state. Furthermore, we analyze the dependence of magic detuning on polarization angle. At magic angle, the magic detuning is independent of the magnetic levels, and the contribution of tensor polarizability is zero. Then, we study and obtain the relationship between magic detuning and principal quantum number of the Rydberg state under the conditions of the magic angle.

## 2. Calculation Methods

With an external electric field, the atomic energy levels split, which is known as the Stark effect. According to the second-order Stark effect [24], the dynamic Stark shift  $\Delta E$  of atoms can be written as

$$\Delta E = -\frac{1}{2}\alpha_i(\omega)F^2 \quad (1)$$

where  $F$  is the alternating electric field;  $\alpha_i(\omega)$  is the dynamic polarizability, which describes the degrees of deviation from the normal distribution of electron clouds of atoms and molecules due to the effect of external fields. When the energy level shifts of the ground state and the excited state are the same at a certain laser frequency, the differential light shift of the transition between the two states is canceled. The trapping laser wavelength at

this time is called the magic wavelength. When  $\omega \neq 0$ , the static polarizability becomes dynamic polarizability, as follows [25]:

$$\alpha_i(\omega) = \alpha_i^S(\omega) + A \cos \theta_k \frac{m_{j_i}}{2j_i} \alpha_i^V(\omega) + \left( \frac{3\cos^2\theta_p - 1}{2} \right) \frac{3m_{j_i}^2 - j_i(j_i + 1)}{j_i(2j_i - 1)} \alpha_i^T(\omega) \quad (2)$$

where  $A$  represents the degree of circular polarization.  $j$  and  $m_j$  represent the total angular momentum quantum number and magnetic quantum number, respectively. As shown in Figure 1,  $\theta_k$  represents the angle between the direction of wave vector  $\hat{k}$  and the quantized axis  $\hat{e}_z$ , which satisfies the relation  $\cos \theta_k = \hat{k} \cdot \hat{e}_z$ .  $\theta_p$ , is related to the direction of polarization vector  $\hat{e}$  and quantization axis  $\hat{e}_z$ .  $\theta_p$  is determined by the geometric relations

$$\cos^2\theta_p = \cos^2\psi \cos^2\theta_{maj} + \sin^2\psi \cos^2\theta_{min} \quad (3)$$

where  $\theta_{maj}$  is the angle between the major axis of the ellipse and the quantized axis, and  $\theta_{min}$  is the angle between the minor semi-axis of the ellipse and the quantized axis. At the same time,  $\theta_p$  and  $\theta_k$  are required to satisfy the geometric relation  $\cos^2\theta_k + \cos^2\theta_p \leq 1$ .  $\psi$  is related to the degree of polarization and satisfies the relation of  $A = \sin 2\psi$ .

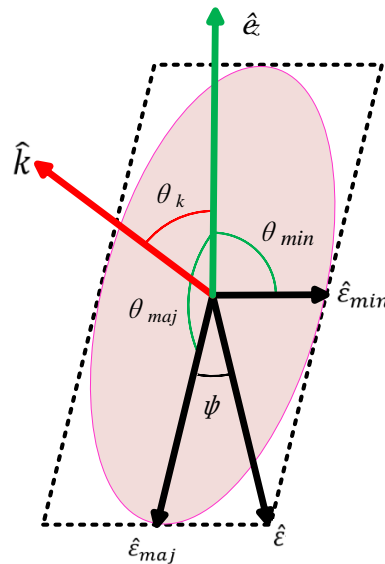


**Figure 1.** The geometrical parameters of electromagnetic plane waves.  $\hat{k}$ ,  $\hat{e}_z$ , and  $\hat{e}$  are the unit wave vector, the quantized axis, and the laser polarization vector, respectively. The parameters  $\theta_{maj}$ ,  $\theta_{min}$ , and  $\theta_k$  are the angles between each unit vector and the quantized axis.

For the expressions of dynamic polarizability in Equation (2),  $\alpha_i^S(\omega)$ ,  $\alpha_i^V(\omega)$ , and  $\alpha_i^T(\omega)$  represent scalar, vector, and tensor polarizabilities, respectively, which are expressed as

$$\begin{aligned} \alpha_i^S(\omega) &= \sum_n \frac{f_{in}}{\Delta E_{ni}^2 - \omega^2} \\ \alpha_i^V(\omega) &= -3 \sqrt{\frac{6j_i(2j_i + 1)}{j_i + 1}} \sum_n (-1)^{j_n + j_i} \left\{ \begin{matrix} 1 & 1 & 1 \\ j_i & j_i & j_n \end{matrix} \right\} \frac{f_{in}}{\Delta E_{ni}^2 - \omega^2} \cdot \frac{\omega}{\Delta E_{ni}} \\ \alpha_i^T(\omega) &= 6 \sqrt{\frac{5j_i(2j_i - 1)(2j_i + 1)}{6(j_i + 1)(2j_i + 3)}} \sum_n (-1)^{j_n + j_i} \left\{ \begin{matrix} 1 & 1 & 2 \\ j_i & j_i & j_n \end{matrix} \right\} \frac{f_{in}}{\Delta E_{ni}^2 - \omega^2} \end{aligned} \quad (4)$$

The oscillator strength is defined as

$$f_{in} = \frac{2\Delta E_{ni}}{3(2j_i + 1)} \left| \langle \Psi_i \| r C^1(\hat{r}) \| \Psi_n \rangle \right|^2 \quad (5)$$

where  $\Delta E_{ni} = E_n - E_i$  and  $\langle \Psi_i || r C^1(\hat{r}) || \Psi_n \rangle$  are the transition energy and the reduced matrix element from the  $|\Psi(n)\rangle$  state to the  $|\Psi(i)\rangle$  state, respectively.  $C^1(\hat{r})$  is the first-order spherical tensor. These values can be found from Reference [26].

Here, we utilize the sum-over-states method [27] to determine the atomic polarizability. The sum-over-states method uses a straightforward interpretation of Equation (4) with the contribution from each state  $n$ , which is determined individually. For Equation (2), when the total angular momentum is less than 1, the tensor polarizability does not exist. When  $A = 0$  corresponds to the linearly polarized light, the dynamic polarizability can be expressed as

$$\alpha_i(\omega) = \alpha_i^S(\omega) + \left( \frac{3\cos^2\theta_p - 1}{2} \right) \frac{3m_{j_i}^2 - j_i(j_i + 1)}{j_i(2j_i - 1)} \alpha_i^T(\omega) \tag{6}$$

### 3. Results and Discussion

#### 3.1. Magic Condition for Cs $6S_{1/2}$ Ground State and $70P_{3/2}$ Rydberg State

In an ODT formed by a single-mode Gaussian beam, the trapping potential depth  $U$  is proportional to the atomic polarizability  $\alpha_i(\omega)$  with opposite signs, as follows:

$$U = -\frac{I(r)}{2\epsilon_0 c} \alpha_i(\omega) \tag{7}$$

where  $I(r)$ ,  $\epsilon_0$ , and  $c$  are the laser intensity profile, the permittivity, and the speed of light in a vacuum, respectively. When the frequency of the laser field is red-detuned to the atomic resonant transition, the polarizability of the ground state is greater than zero, so the atoms are attracted to the maximum light intensity. On the contrary, the loosely bound Rydberg-state electron is almost “free”, and its polarizability  $\alpha_{nP_{3/2}}(\omega) \approx -e^2 / (m_e \omega^2)$  is negative [28], so Rydberg atoms will be pushed towards the minimum light intensity. Therefore, the conventional far-off-resonance red-detuned ODT is a potential well for the ground state but is a potential barrier for the Rydberg state, which will accelerate the Rydberg atom away from its original position, as shown in Figure 2a. However, the trapping potential of the  $|g\rangle$  and  $|r\rangle$  states can be equalized when an ODT laser is tuned to the blue side of the  $|r\rangle \leftrightarrow |a\rangle$  auxiliary transition, where the trap are the attractive potential for the ground and Rydberg states, as shown in Figure 2b.

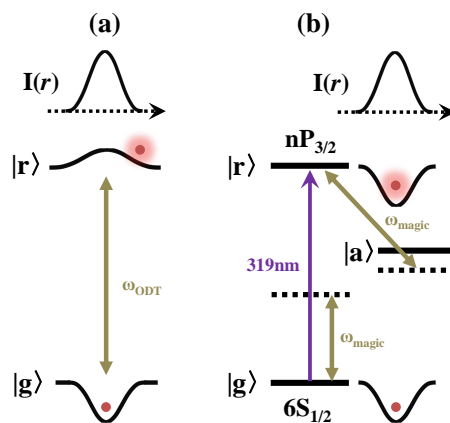


**Figure 2.** Trapping of Rydberg atoms. (a) The conventional far-off-resonance red-detuned ODT is attractive for ground states but usually repulsive for highly excited Rydberg states. (b) The direct single-photon transition from  $|g\rangle = |6S_{1/2}\rangle$  to  $|r\rangle = |nP_{3/2}\rangle$  coupled by a 319-nm ultraviolet laser. The trapping potential of the  $|g\rangle$  and  $|r\rangle$  states can be equalized when an ODT laser is tuned to the blue side of the  $|r\rangle \leftrightarrow |a\rangle$  auxiliary transition.

First, we consider two particular cases for linearly polarized light, the polarizability contains only scalar and tensor parts from Equation (6). One of them is  $|\cos \theta_p|^2 = 1$ , which means the  $\hat{e}_z$  axis is perpendicular to the wave vector but parallel to the polarization vector ( $\hat{e}_z \perp \hat{k}$  and  $\hat{e}_z \parallel \hat{\epsilon}$ ). Thus, Equation (6) is written as

$$\alpha_i(\omega) = \alpha_i^S(\omega) + \frac{3m_{ji}^2 - j_i(j_i + 1)}{j_i(2j_i - 1)}\alpha_i^T(\omega) \tag{8}$$

Another case is  $|\cos \theta_p|^2 = 0$ , which means the  $\hat{e}_z$  axis is perpendicular to the wave vector and the polarization vector ( $\hat{e}_z \perp \hat{k}$  and  $\hat{e}_z \perp \hat{\epsilon}$ ). Thus, Equation (6) can be written as

$$\alpha_i(\omega) = \alpha_i^S(\omega) - \frac{3m_{ji}^2 - j_i(j_i + 1)}{j_i(2j_i - 1)}\alpha_i^T(\omega) \tag{9}$$

Figure 3 is the dynamic polarizabilities of  $6S_{1/2}$  (red dashed lines) and  $70P_{3/2}$  (blue and black solid lines) states in the case of linearly polarized light, where the quantized axis is parallel to the polarization plane ( $\hat{e}_z \parallel \hat{\epsilon}$ ). In the range of 600–2000 nm, there are six magic wavelengths corresponding to the following auxiliary transitions of  $70P_{3/2} \leftrightarrow 7S_{1/2}$ ,  $70P_{3/2} \leftrightarrow 6D_{5/2,3/2}$ ,  $70P_{3/2} \leftrightarrow 8S_{1/2}$ , and  $70P_{3/2} \leftrightarrow 7D_{5/2,3/2}$ . For the  $70P_{3/2} \leftrightarrow 7S_{1/2}$  auxiliary transition, the potential is repulsive for the ground and Rydberg states in the crossing point of the dynamic polarizabilities, so it is not considered.

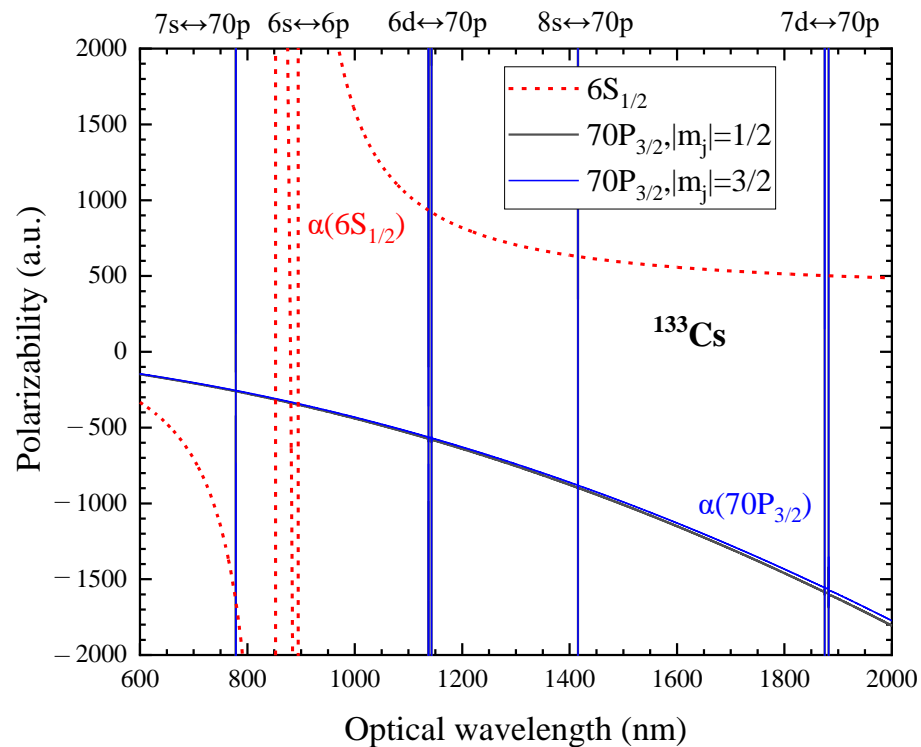


**Figure 3.** Dynamic polarizabilities of Cs  $6S_{1/2}$  ground state (red dashed lines) and  $70P_{3/2}$  Rydberg state (blue and black solid lines) between 600 nm and 2000 nm.

The dynamic polarizabilities of  $6S_{1/2}$  ground state and  $70P_{3/2}$  Rydberg state near the  $70P_{3/2} \leftrightarrow 7D_{5/2}$  auxiliary transition are shown in Figure 4. The upper part is quantized axis in the plane of the vertical polarization, the lower part is quantized axis parallel to the polarization plane (A partial enlargement of Figure 3). The polarizability curves of the  $6S_{1/2}$  ground state and  $70P_{3/2}$  Rydberg state intersect at two points, corresponding to the transitions of  $6S_{1/2} \leftrightarrow 70P_{3/2}$  ( $|m_j| = 1/2$ ) and  $6S_{1/2} \leftrightarrow 70P_{3/2}$  ( $|m_j| = 3/2$ ). The

wavelength at the intersection point is called the magic wavelength, where the potential depth of the magic-wavelength ODT is equal for the ground-state and Rydberg-state atoms.

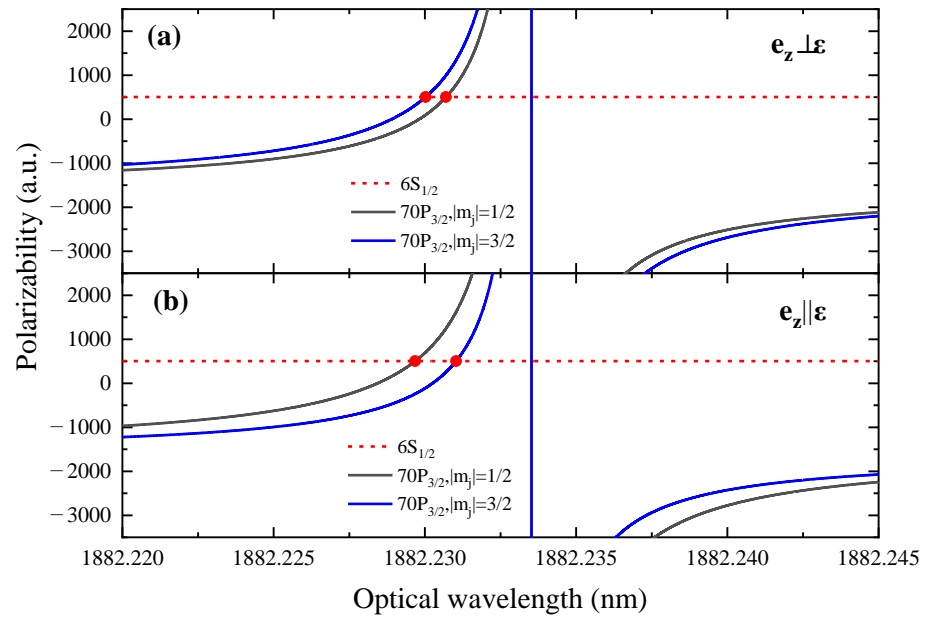


**Figure 4.** The dynamic polarizabilities of the ground state and the Rydberg state in the case of linearly polarized light in the range from 1882.220 to 1882.245 nm near the auxiliary transition of  $70P_{3/2} \leftrightarrow 7D_{5/2}$ . (a) The quantization axis is perpendicular to the plane of polarization and (b) the quantization axis is parallel to the plane of polarization.

Figure 4 shows that the dynamic polarizability of the  $6S_{1/2}$  ground state is almost the same, but that of the  $70P_{3/2}$  excited state is not the same in different polarization angles  $\theta_p$ . Specifically, its change is very dramatic near the resonance position. Therefore, it is necessary to study the magic wavelength as the change in polarization angle. Because the difference between the magic wavelength and the auxiliary transition wavelength is only a few picometers to tens of picometers, it is more intuitive to exhibit a change in magic detuning with the polarization angle.

In Figure 5, the simulation results show that the magic detuning as the change in polarization angle is a linear near magic wavelength for all auxiliary transitions of  $70P_{3/2} \leftrightarrow 7D_{5/2}$ ,  $70P_{3/2} \leftrightarrow 8S_{1/2}$ , and  $70P_{3/2} \leftrightarrow 6D_{5/2}$ , and the range is finite, not exceeding 1 GHz. For the  $6S_{1/2} \leftrightarrow 70P_{3/2}$  ( $|m_j| = 1/2$ ) transition, the magic detuning increases with an increase in the polarization angle, but for the  $6S_{1/2} \leftrightarrow 70P_{3/2}$  ( $|m_j| = 3/2$ ) transition, the magic detuning decreases with the increase in polarization angle. Therefore, the magic condition is very sensitive to the polarization angle due to the contribution of anisotropic tensor polarizability. For any magic condition of the auxiliary transitions of  $70P_{3/2} \leftrightarrow 7D_{5/2}$ ,  $70P_{3/2} \leftrightarrow 8S_{1/2}$ , and  $70P_{3/2} \leftrightarrow 6D_{5/2}$ , different curves intersect at one point. At this point, the magic detuning is independent of the magnetic levels, and the contribution of tensor polarizability is zero. In this case, the polarization angle satisfies the condition of  $|\cos \theta_p|^2 = 1/3$  for linearly polarized light. This polarization angle  $\theta_p$  is referred to as a “magic angle” and is given by [29]

$$\theta_p = \arccos\left(1/\sqrt{3}\right) = 54.7^\circ \tag{10}$$

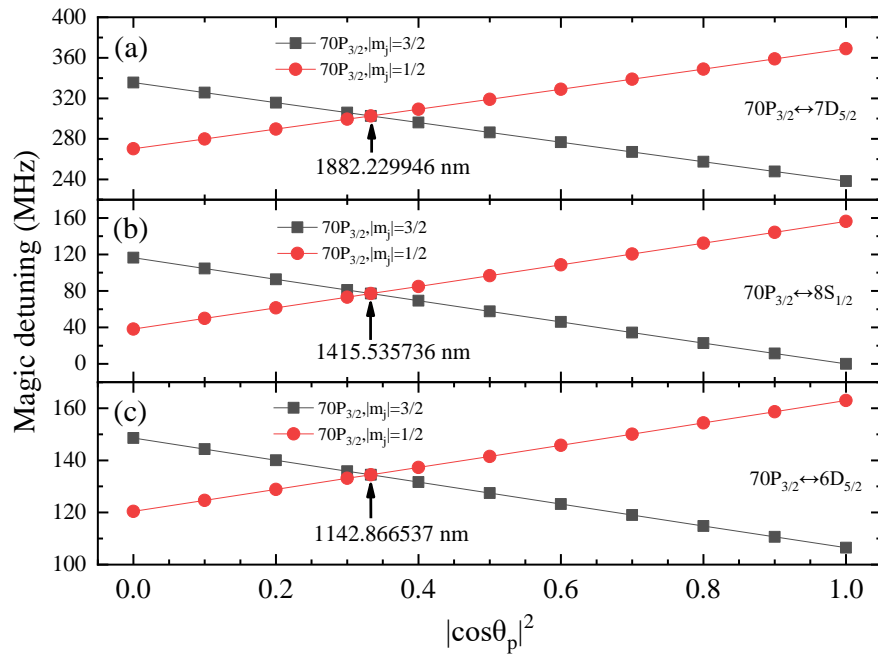


**Figure 5.** The dependence of magic detuning for the  $6S_{1/2} \leftrightarrow 70P_{3/2}$  transition near different auxiliary transitions on  $|\cos \theta_p|^2$  in the case of linearly polarized light. (a)  $70P_{3/2} \leftrightarrow 7D_{5/2}$  auxiliary transition; (b)  $70P_{3/2} \leftrightarrow 8S_{1/2}$  auxiliary transition; (c)  $70P_{3/2} \leftrightarrow 6D_{5/2}$  auxiliary transition.

To be specific, the magic detunings at the magic angle are 302.67 MHz for the  $70P_{3/2} \leftrightarrow 7D_{5/2}$  auxiliary transition, 77.08 MHz for the  $70P_{3/2} \leftrightarrow 8S_{1/2}$  auxiliary transition, and 134.48 MHz for the  $70P_{3/2} \leftrightarrow 6D_{5/2}$  auxiliary transition, and the corresponding magic wavelengths are 1882.229946, 1415.535736, and 1142.866537 nm for the  $6S_{1/2} \leftrightarrow 70P_{3/2}$  transition, which are listed in Table 1. These magic ODTs can be implemented by combining an ultra-stable optical cavity and a master oscillator power-amplifier (MOPA) system, which consists of a rare-earth-doped (Thulium, Erbium, and Ytterbium) distributed feedback fiber laser and a corresponding fiber amplifier with watt-level output power. When the watt-level single-mode Gaussian laser beam produced by the MOPA system is strongly focused to the micrometer waist spot, it is easy to form an ODT with mK potential well depth. According to Equation (7), when the atomic polarizability is constant, the potential well depth is proportional to the light intensity. Therefore, when an ODT laser is tuned to the blue side of any auxiliary transition in Figure 6b, the  $6S_{1/2}$  ground-state and  $70P_{3/2}$  Rydberg-state atoms will be confined in the waist spot of a strongly focused single-mode Gaussian laser beam, as shown in Figure 6a.

**Table 1.** At magic angle, magic detunings and magic wavelengths of the  $6S_{1/2} \leftrightarrow 70P_{3/2}$  transition near the  $70P_{3/2} \leftrightarrow 7D_{5/2}$ ,  $70P_{3/2} \leftrightarrow 8S_{1/2}$ , and  $70P_{3/2} \leftrightarrow 6D_{5/2}$  auxiliary transitions.

Auxiliary Transition	Magic Detuning (MHz)	Magic Wavelength (nm)
$70P_{3/2} \leftrightarrow 7D_{5/2}$	302.67	1882.229946
$70P_{3/2} \leftrightarrow 8S_{1/2}$	77.08	1415.535736
$70P_{3/2} \leftrightarrow 6D_{5/2}$	134.48	1142.866537

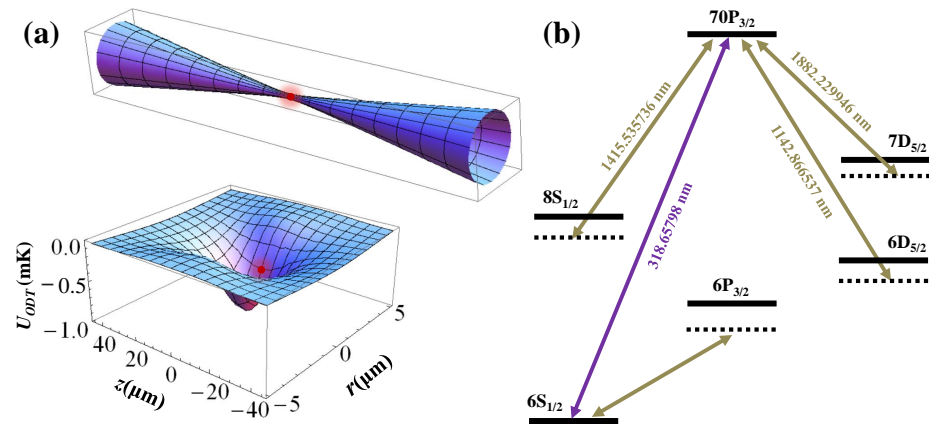


**Figure 6.** (a) A magic ODT formed by a strongly focused single-mode Gaussian laser beam. (b) The involved energy level diagram of magic ODTs for the  $6S_{1/2} \leftrightarrow 70P_{3/2}$  single-photon transition coupled by a 318.65798 nm ultra-violet laser. The brown double arrow lines are auxiliary transitions from  $70P_{3/2}$  to  $7D_{5/2}$ ,  $8S_{1/2}$ , and  $6D_{5/2}$ , and the corresponding magic wavelengths are 1882.229946, 1415.535736, and 1142.866537 nm, respectively.

### 3.2. Magic Trapping Condition for Cs $nP_{3/2}$ Rydberg States

Considering that magic detuning is independent of the magnetic levels at the magic angle, we calculate the magic detuning of the  $6S_{1/2} \leftrightarrow nP_{3/2}$  transition for different principal quantum numbers from  $n = 50$  to  $90$  at that point, as shown in Figure 7. Here, the black squares represent the magic detuning for the  $nP_{3/2} \leftrightarrow 7D_{5/2}$  auxiliary transition. The red circles and blue triangles are the magic detuning for the auxiliary transitions of  $nP_{3/2} \leftrightarrow 8S_{1/2}$  and  $nP_{3/2} \leftrightarrow 6D_{5/2}$ , respectively. In order to establish the relationship between the magic detuning  $\Delta_{magic}$  and the principal quantum number  $n$ , these data are fitted by

$$\Delta_{magic} = a \cdot n^b + c \tag{11}$$

where the coefficients of  $a$ ,  $b$ , and  $c$  are constants, which are determined by fitting the calculated results in Figure 7. Since the atomic polarizability is proportional to  $n^7$ , the polarizability of the atomic state with higher principal quantum number is greater than that of low-excited states, which make it more sensitive to the external electric field. It will result in a larger blue light shift in the higher Rydberg states by the same trapping laser field. In order to compensate for the light shift, it is necessary to increase the coupling intensity between the trapping laser and the auxiliary transition, that is, to reduce the detuning between them. Therefore, to make the target Rydberg state and the ground state reach the same light shift, the larger the principal quantum number is, the smaller the magic detuning is, as shown in Figure 7. The coefficients of  $a$ ,  $b$ , and  $c$  for the auxiliary transitions of  $nP_{3/2} \leftrightarrow 7D_{5/2}$ ,  $nP_{3/2} \leftrightarrow 8S_{1/2}$ , and  $nP_{3/2} \leftrightarrow 6D_{5/2}$  obtained by fitting the calculated results with Equation (11) are listed in Table 2. It can be seen that for any auxiliary transition, the magic detuning decreases exponentially with the principal quantum number, and the exponent  $b$  is basically the same, about 3.324(10). Thus, combined with Equation (11) and Table 2, we can obtain the magic detuning of the  $6S_{1/2} \leftrightarrow nP_{3/2}$  transition corresponding to any auxiliary transition at magic angle, which provides more theoretical basis and support for the subsequent experimental research [30–34] on coherent manipulation of Cs ground-state and Rydberg-state atoms in the magic ODT.

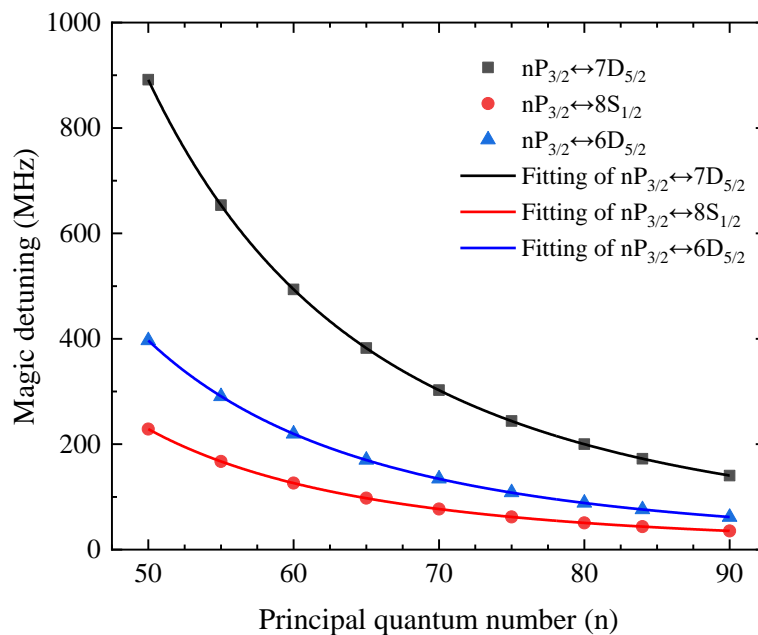


**Figure 7.** In the vicinity of different auxiliary transitions, the magic detuning at magic angle varies with the principal quantum number from 50 to 90. The solid lines are the fitted results.

**Table 2.** The coefficients *a*, *b*, and *c* of Equation (11) for the auxiliary transitions of  $nP_{3/2} \leftrightarrow 7D_{5/2}$ ,  $nP_{3/2} \leftrightarrow 8S_{1/2}$ , and  $nP_{3/2} \leftrightarrow 6D_{5/2}$  which are determined by fitting the results in Figure 7.

Auxiliary Transition	<i>a</i> (MHz)	<i>b</i>	<i>c</i> (MHz)
$nP_{3/2} \leftrightarrow 7D_{5/2}$	$3.881(6) \times 10^8$	3.324(5)	16.6(5)
$nP_{3/2} \leftrightarrow 8S_{1/2}$	$1.050(2) \times 10^8$	3.337(5)	3.9(1)
$nP_{3/2} \leftrightarrow 6D_{5/2}$	$1.653(5) \times 10^8$	3.312(8)	6.1(4)

#### 4. Conclusions

In summary, we performed a calculation about the dynamic polarizabilities of Cs  $6S_{1/2}$  ground state and  $nP_{3/2}$  Rydberg state using the sum-over-states method. Due to the existence of anisotropic tensor parts of atomic states with an angular momentum greater than 1/2, the atomic dynamic polarizabilities are very sensitive to the polarization direction of the laser field. Therefore, the magic wavelength of the transition between two atomic states, at which the differential light shift of the  $6S_{1/2} \leftrightarrow nP_{3/2}$  transition can be canceled, also depends on the polarization angle between the quantized axis and the polarization vector. By introducing an electric dipole auxiliary transition connected the target Rydberg state and the low-excited state, the magic condition of the  $6S_{1/2} \leftrightarrow nP_{3/2}$  transition of Cs atoms is determined by the intersection of dynamic polarizabilities of the two states. Because the frequency difference between the auxiliary transition and the magic laser field is relatively small, only a few hundred MHz, we analyze the dependence of magic detuning on the polarization angle. There exists a magic angle where the magic detuning does not depend on the magnetic levels, and the contribution of tensor polarizability is zero. Under the condition of the magic angle, the relationship between magic detuning and the principal quantum number of the Rydberg state has been established. It will provide more theoretical basis and support for the subsequent experimental research on the trapping and coherent manipulation of the ground-state and Rydberg-state atoms in the magic light trap.

**Author Contributions:** Conceptualization, methodology, and investigation, J.B. and J.W.; software, J.B.; validation, formal analysis, data administration, and visualization, X.W. and X.H.; writing—original draft preparation, J.B.; writing—review and editing, J.W.; resources, supervision, project administration, and funding acquisition, J.B., W.L. and J.W. All authors have read and agreed to the published version of the manuscript.

**Funding:** This research was funded by the National Key R & D Program of China (2021YFA1402002), the National Natural Science Foundation of China (12104417 and 12104419), and the Fundamental Research Program of Shanxi Province (20210302124161 and 20210302124689).

**Institutional Review Board Statement:** Not applicable.

**Informed Consent Statement:** Not applicable.

**Data Availability Statement:** The data that support the findings of this study are available from the first author and the corresponding author upon reasonable request.

**Conflicts of Interest:** The authors declare no conflicts of interest.

## References

1. Gallagher, T.F. *Rydberg Atoms*; Cambridge University Press: Cambridge, UK, 2005.
2. Saffman, M.; Walker, T.G.; Mølmer, K. Quantum information with Rydberg atoms. *Rev. Mod. Phys.* **2010**, *82*, 2313–2363. [[CrossRef](#)]
3. Adams, C.S.; Pritchard, J.D.; Shaffer, J.P. Rydberg atom quantum technologies. *J. Phys. B At. Mol. Opt. Phys.* **2020**, *53*, 012002. [[CrossRef](#)]
4. Browaeys, A.; Lahaye, T. Many-body physics with individually controlled Rydberg atoms. *Nat. Phys.* **2020**, *16*, 132–142. [[CrossRef](#)]
5. Dudin, Y.O.; Kuzmich, A. Strongly interacting Rydberg excitations of a cold atomic gas. *Science* **2012**, *336*, 887. [[CrossRef](#)]
6. Ripka, F.; Kübler, H.; Löw, R.; Pfau, T. A room-temperature single-photon source based on strongly interacting Rydberg atoms. *Science* **2018**, *362*, 446–449. [[CrossRef](#)]
7. Gorniaczyk, H.; Tresp, C.; Schmidt, J.; Fedder, H.; Hofferberth, S. Single-photon transistor mediated by interstate Rydberg interactions. *Phys. Rev. Lett.* **2014**, *113*, 053601. [[CrossRef](#)]
8. Urban, E.; Johnson, T.A.; Henage, T.; Isenhower, L.; Yavuz, D.D.; Walker, T.G.; Saffman, M. Observation of Rydberg blockade between two atoms. *Nat. Phys.* **2009**, *5*, 110–114. [[CrossRef](#)]
9. Sun, L.N.; Yan, L.L.; Su, S.L.; Jia, Y. One-step implementation of time-optimal-control three-qubit nonadiabatic holonomic controlled gates in Rydberg atoms. *Phys. Rev. Appl.* **2021**, *16*, 064040. [[CrossRef](#)]
10. Grimm, R.; Weidemüller, M.; Ovchinnikov, Y.B. Optical dipole traps for neutral atoms. *Adv. At. Mol. Opt. Phys.* **2000**, *42*, 95–170. [[CrossRef](#)]
11. Choi, J.H.; Guest, J.R.; Povilus, A.P.; Hansis, E.; Raithel, G. Magnetic trapping of long-lived cold Rydberg atoms. *Phys. Rev. Lett.* **2005**, *95*, 243001. [[CrossRef](#)]
12. Boetes, A.G.; Skannrup, R.V.; Naber, J.; Kokkelmans, S.J.J.M.F.; Spreeuw, R.J.C. Trapping of Rydberg atoms in tight magnetic microtraps. *Phys. Rev. A* **2018**, *97*, 013430. [[CrossRef](#)]
13. Hogan, S.D.; Merkt, F. Demonstration of three-dimensional electrostatic trapping of state-selected Rydberg atoms. *Phys. Rev. Lett.* **2008**, *100*, 043001. [[CrossRef](#)]
14. Anderson, S.E.; Younge, K.C.; Raithel, G. Trapping Rydberg atoms in an optical lattice. *Phys. Rev. Lett.* **2011**, *107*, 263001. [[CrossRef](#)]
15. Barredo, D.; Lienhard, V.; Scholl, P.; de Léséleuc, S.; Boulier, T.; Browaeys, A.; Lahaye, T. Three-dimensional trapping of individual Rydberg atoms in ponderomotive bottle beam traps. *Phys. Rev. Lett.* **2020**, *124*, 023201. [[CrossRef](#)]
16. Cortiñas, R.G.; Favier, M.; Ravon, B.; Méhaignerie, P.; Machu, Y.; Raimond, J.M.; Sayrin, C.; Brune, M. Laser trapping of circular Rydberg atoms. *Phys. Rev. Lett.* **2020**, *124*, 123201. [[CrossRef](#)]
17. McKeever, J.; Buck, J.R.; Boozer, A.D.; Kuzmich, A.; Nagerl, H.C.; Stamper-Kurn, D.M.; Kimble, H.J. State-insensitive cooling and trapping of single atoms in an optical cavity. *Phys. Rev. Lett.* **2003**, *90*, 133602. [[CrossRef](#)]
18. Li, L.; Dudin, Y.O.; Kuzmich, A. Entanglement between light and an optical atomic excitation. *Nature* **2013**, *498*, 466–469. [[CrossRef](#)]
19. Bai, J.D.; Liu, S.; He, J.; Wang, J.M. Towards implementation of a magic optical-dipole trap for confining ground-state and Rydberg-state cesium cold atoms. *J. Phys. B At. Mol. Opt. Phys.* **2020**, *53*, 155302. [[CrossRef](#)]
20. Wilson, J.T.; Saskin, S.; Meng, Y.; Ma, S.; Dilip, R.; Burgers, A.P.; Thompson, J.D. Trapping alkaline earth Rydberg atoms optical tweezer arrays. *Phys. Rev. Lett.* **2022**, *128*, 033201. [[CrossRef](#)]
21. Mei, Y.; Li, Y.; Nguyen, H.; Berman, P.; Kuzmich, A. Trapped alkali-metal Rydberg qubit. *Phys. Rev. Lett.* **2022**, *128*, 123601. [[CrossRef](#)]
22. Wang, J.M.; Guo, S.L.; Ge, Y.L.; Cheng, Y.J.; Yang, B.D.; He, J. State-insensitive dichromatic optical-dipole trap for rubidium atoms: calculation and the dichromatic laser's realization. *J. Phys. B At. Mol. Opt. Phys.* **2014**, *47*, 095001. [[CrossRef](#)]

23. Liu, B.; Jin, G.; Sun, R.; He, J.; Wang, J.M. Measurement of magic-wavelength optical dipole trap by using the laser-induced fluorescence spectra of trapped single cesium atoms. *Opt. Express* **2017**, *25*, 15861–15867. [[CrossRef](#)] [[PubMed](#)]
24. Zimmerman, M.L.; Littman, M.G.; Kash, M.M.; Kleppner, D. Stark structure of the Rydberg states of alkali-metal atoms. *Phys. Rev. A* **1979**, *20*, 2251–2275. [[CrossRef](#)]
25. Kien, F.L.; Schneeweiss, P.; Rauschenbeutel, A. Dynamical polarizability of atoms in arbitrary light fields: general theory and application to cesium. *Eur. Phys. J. D* **2013**, *67*, 92. [[CrossRef](#)]
26. Šibalić, N.; Pritchard, J.D.; Adams, C.S.; Weatherill, K.J. ARC: An open-source library for calculating properties of alkali Rydberg atoms. *Comput. Phys. Commun.* **2017**, *220*, 319–331. [[CrossRef](#)]
27. Mitroy, J.; Safronova, M.S.; Clark, C.W. Theory and applications of atomic and ionic polarizabilities. *J. Phys. B At. Mol. Opt. Phys.* **2010**, *43*, 202001. [[CrossRef](#)]
28. Younge, K.C.; Anderson, S.E.; Raithel, G. Adiabatic potentials for Rydberg atoms in a ponderomotive optical lattice. *New J. Phys.* **2010**, *12*, 023031. [[CrossRef](#)]
29. Budker, D.; Kimball, D.; DeMille, D. *Atomic Physics: An Exploration through Problems and Solutions*; Oxford University Press: Oxford, UK, 2010.
30. Hankin, A.M.; Jau, Y.Y.; Parazzoli, L.P.; Chou, C.W.; Armstrong, D.J.; Landahl, A.J.; Biedermann, G.W. Two-atom Rydberg blockade using direct  $6S$  to  $nP$  excitation. *Phys. Rev. A* **2014**, *89*, 033416. [[CrossRef](#)]
31. Jau, Y.Y.; Hankin, A.M.; Keating, T.; Deutsch, I.H.; Biedermann, G.W. Entangling atomic spins with a Rydberg-dressed spin-flip blockade. *Nat. Phys.* **2015**, *12*, 71–74. [[CrossRef](#)]
32. Wang, J.Y.; Bai, J.D.; He, J.; Wang, J.M. Single-photon cesium Rydberg excitation spectroscopy using 318.6-nm UV laser and room-temperature vapor cell. *Opt. Express* **2017**, *25*, 22510–22518. [[CrossRef](#)]
33. Bai, J.D.; Wang, J.Y.; Liu, S.; He, J.; Wang, J.M. Autler–Townes doublet in single-photon Rydberg spectra of cesium atomic vapor with a 319 nm UV laser. *Appl. Phys. B* **2019**, *125*, 33. [[CrossRef](#)]
34. Bai, J.D.; Liu, S.; Wang, J.Y.; He, J.; Wang, J.M. Single-photon Rydberg excitation and trap-loss spectroscopy of cold cesium atoms in a magneto-optical trap by using of a 319-nm ultraviolet laser system. *IEEE J. Sel. Top. Quant. Electr.* **2020**, *26*, 1600106. [[CrossRef](#)]